



PDO influenced interdecadal summer precipitation change over East China in mid-18th century



Gebanruo Chen^{1,2,3}, Xiangyu Li^{1,4}✉, Zhiqing Xu⁵, Yong Liu^{1,4}, Zhongshi Zhang^{1,4}, Shiyu Shao¹ & Jing Gao²

There have been few case studies of the relationship between the Pacific Decadal Oscillation (PDO) and the East Asian climate before the pre-industrial era with limited anthropogenic impacts. Using the CESM Last Millennium Ensemble (CESM-LME) simulation with reconstruction evidence, we showed that there was an interdecadal transition of the summer precipitation in East China, with the pattern of “southern flooding and northern drought” in the mid-18th century. The interdecadal transition was influenced by PDO, as suggested by both the reconstruction evidence and simulation. Corresponding to the positive PDO phase change, the East Asia-Pacific pattern teleconnection wave train propagated northward and modulated the circulation and precipitation in East China, together with the southward movement of the East Asian westerly jet. The volcanic double or clustered eruptions are thought to have played a crucial role on the shift of the PDO phase and the decadal summer climate change over East China during the mid-18th century. Incorporating volcanic activity in a reasonable manner would likely improve decadal simulations of East Asian climate in the past and predictions in the future.

Investigating and predicting interdecadal climate change is a challenging endeavor and constitutes a fundamental aspect of the International Coupled Model Intercomparison Project Phase Six^{1–3}. However, our understanding of the factors and mechanisms driving the interdecadal climate change, particularly concerning the Asian summer monsoon, remains limited⁴. In comparison to other time scales, the temporal evolution and spatial patterns of the Asian summer monsoon at interdecadal scales exhibit greater uncertainties^{4–7}. The interdecadal variation of summer precipitation in East China is influenced by both internal variability within the climate system and external forcing factors. These external factors include increases in greenhouse gases, anthropogenic land cover change, volcanic eruptions, and solar irradiation. The external forcing could also influence the internal variability, such as Pacific Decadal Oscillation (PDO) and Atlantic Multidecadal Variability^{8–13}. These external factors contribute to the complex interplay that shapes the interdecadal variability of the Asian summer monsoon and its associated precipitation patterns in East China.

The PDO is an internal variability that significantly influences the interdecadal variation of summer precipitation in East China^{6,14–17}, through teleconnections originating from tropical and mid-to-high latitudes. The PDO-related sea surface temperature (SST) anomalies trigger subsequent

changes in tropical convection and precipitation, which can impact the climate pattern in East Asia through a meridional wave train of Pacific-Japan or East Asia-Pacific^{18–23}. Additionally, the PDO can influence the interdecadal summer precipitation over East China through teleconnection wave trains at mid-to-high latitudes along the Asian westerly waveguide. This influence is dependent on the stage evolution of the PDO and can be altered by the phase of Atlantic Multidecadal Oscillation^{16,21,23–26}. Furthermore, the PDO can also modulate the intensity of the westerly jet^{18,27} and the Western North Pacific subtropical high²⁰, thereby affecting the interdecadal summer precipitation in East China.

However, it is important to note that internal climate variability factors like the PDO can also be influenced by external forcing factors, such as changes in greenhouse gas concentrations^{9,28–34}. In response to variations in CO₂ concentration that induce global warming or cooling induced, the amplitude of the PDO can undergo significant alternations. These changes occur due to alternations in the meridional temperature gradient and air-sea feedback^{9,31,35}. Additionally, the time scale of PDO can vary due to changes in the intensity of ocean stratification and phase speed of internal Rossby waves⁹. The influence of CO₂ fluctuation on the PDO suggests that our current understanding of the relationship between the PDO and the East

¹Department of Atmospheric Science, School of Environmental Studies, China University of Geosciences, Wuhan 430074, China. ²State Key Laboratory of Tibetan Plateau Earth System, Environment and Resources (TPESER), Institute of Tibetan Plateau Research, Chinese Academy of Sciences, Beijing 100101, China.

³University of Chinese Academy of Sciences, Beijing 100049, China. ⁴Centre for Severe Weather and Climate and Hydro-geological Hazards, Wuhan 430074, China. ⁵Institute of Atmospheric Physics, Chinese Academy of Sciences, Beijing 100029, China. ✉e-mail: lixiangyu@cug.edu.cn

Asian monsoon is based on a combination of external forcing, such as greenhouse gases, internal variability, and the modulation of external forcing on the internal variability. This highlights the complex interplay between external forcing factors and internal climate variability in shaping the behavior of the PDO and its connection to the East Asian monsoon.

Prior to the pre-industrial era, human activities had a minimal impact on the climate, and anthropogenic greenhouse gas emissions were negligible^{36,37}. The concentration of atmosphere CO₂ was low and exhibited minimal variation, which had a negligible effect on the internal variability of the climate system. Recent studies have placed growing emphasis on comprehending the variance of the internal variability, including PDO and Atlantic Multidecadal Oscillation, and their correlation with East Asian climate over the last millennium^{10,26,33,38–46}. This understanding is primarily achieved through simulations and statistical analyses conducted during typical periods. However, there are still a limited number of case studies investigating the relationship between internal variability and East Asian climate before the pre-industrial era. Here, we combined simulation and reconstruction⁴¹ to investigate the interdecadal change of summer precipitation over East China in the 18th century and its relationship with PDO. In particular, the interdecadal transition of the summer precipitation in East China in the mid-18th century was found to be strongly associated with changes in the PDO phase. The study highlights that volcanic activity may have played a crucial role in the shift of the PDO phase during the mid-18th century.

Results

Interdecadal change around 1760 A.D.

Based on reconstruction, the summer precipitation over North China (34°–43°N, 107.5°–122°E) underwent interdecadal fluctuations (Fig. 1a), with significant changes around 1750 A.D. and 1758 A.D. as determined by sliding t test (Supplementary Figure 1a). Over southern China (22°–30°N, 105.5°–122°E), the summer precipitation also depicted interdecadal variations (Fig. 1c), with noteworthy change around 1760 A.D. according to sliding t test (Supplementary Figure 1b). Overall, around 1760 A.D., there was an interdecadal change in the summer climate over East China, with contrasting patterns observed between North China and Southern China. North China transitioned from a wet phase to a dry phase, while southern China experienced a shift from dry to wet conditions (Fig. 1e).

Focusing on the interdecadal summer precipitation change around 1760 A.D., only ensemble 001 of CESM-LME was able to replicate the interdecadal change in both North China and Southern China (Supplementary Figures 2 and 3). For ensemble 001, there was a significant sliding correlation between reconstructed and simulated summer precipitation around 1760 A.D. in both southern and North China (Supplementary Figures 5 and 6). In contrast to the reconstructed precipitation in East China around 1760 A.D., the interdecadal variations were poorly replicated by PMIP3 models (Supplementary Figures 7–9). As CESM-LME ensemble 001 well reproduced the interdecadal summer precipitation changes in East China around 1760 A.D. (Fig. 1a–d), further analysis will be mainly based on CESM-LME ensemble 001.

Mechanisms of the interdecadal change around 1760 A.D.

Associated with the interdecadal shift around 1760 AD, a notable anomalous cyclone with low pressure centered in South Japan, brought northerly anomalies and cold advection to North China. This led to lower temperatures and reduced water vapor transport (Figs. 2a and 3b). Meanwhile, an anticyclone anomaly emerged in the subtropical region of the Western North Pacific (Fig. 2b–d), strengthening and shifting the subtropical high southward (Fig. 2e–f). As a result, southwest winds and water vapor transport increased in southern China. Simultaneously, the East Asian jet stream shifted southward (Fig. 3c), resulting in anomalous subsidence in North China and anomalous uplift in Southern China (Figs. 3a, c). Consequently, the decrease in water vapor transport and anomalous subsidence (Figs. 3a and 3b) led to reduced summer rainfall in North China, while the

convergence of water vapor and anomalous upward motion (Fig. 3b, 3c) contributed to increased summer rainfall in southern China.

Discussions

During the interdecadal climate change around 1760 A.D., the simulation indicated a positive phase PDO-like SST change, with warmer conditions in the North Pacific subpolar region and the ocean along the coast of North America, and cooler conditions in the interior North Pacific Ocean (Fig. 4a). These changes bear resemblance to the positive phase of the PDO pattern. The simulated positive phase PDO-like SST change around 1760 A.D. is supported by several geological evidences (Fig. 4a and Supplementary Figure 10). After 1760 A.D., reconstructed data show interdecadal increases in SST over the Northeast Pacific⁴⁷ and near the Aleutian Islands⁴⁸. Additionally, the reconstructed warming in the Gulf of Alaska^{49,50} and near the Pacific coast of Kunashir Island⁵¹ (Supplementary Figure 10) corroborate the simulated warming along the North Pacific coast in the subpolar region (Fig. 4a). Moreover, the reconstructed interdecadal SST cooling based on coral archives over the western Pacific⁵² and around Japan's Amami Island⁵³ align with the simulated cooling in the interior North Pacific Ocean (Fig. 4a). Furthermore, the simulated shift of the PDO to a positive phase around 1760 A.D. generally aligns with most reconstructions of PDO indices^{54–59} (Fig. 5a–k), although several paleo-PDO indices suggest a different cold phase^{60–62} (Fig. 5c, d, i) or indicate insignificant variation^{63,64} (Fig. 5e, h). In response to the positive phase PDO-like SST change around 1760 A.D., the warm anomaly over the central and eastern subtropical North Pacific led to the weakening of the zonal SST gradient and Walker circulation. Additionally, the Philippine Sea experienced cooling and the turbulent heat flux reduced there (Fig. 4a, b). As a consequence, convective circulation was impeded, leading to decreased precipitation and latent heating over the ocean to the east of the Philippine (Supplementary Figure 4a). The anomalous latent heating over the east of the Philippine caused the northward propagation of the East Asia-Pacific teleconnection wave train (Fig. 4c and Supplementary Figure 11). This is responsible for the development of the anomalous anticyclone over the subtropical region of the Western North Pacific and the anomalous cyclone located at South Japan (Fig. 2 and 4c). Accordingly, the Western North Pacific subtropical high strengthened and shifted southward, promoting the southwesterly wind anomaly in southern China (Fig. 2). Consequently, warm advection occurred (Fig. 2a), and water vapor transport increased (Fig. 3b). Meanwhile, the anomalous cyclone centered at South Japan generated northerly wind anomalies in North China (Figs. 2a–d), bringing in cold advection and reducing water vapor transport (Fig. 3b). Concurrently, it is noteworthy that the East Asian subtropical westerly jet migrated southwards, causing anomalous uplift in the south and anomalous subsidence in the north (Fig. 3a, 3c). Taken together, the decrease in northward water vapor transport flux, along with anomalous divergence and subsidence, contributed to the reduction in precipitation in North China. Simultaneously, the rise in water vapor transport flux, in combination with anomalous convergence and upward motion, resulted in the precipitation increase in southern China. Notably, the North Atlantic region became cooling over the 0–50°N and warming north of the 50°N, resembling the negative phase of Atlantic Multidecadal Oscillation around 1760 A.D. This pattern was accompanied by the propagation of a zonal Rossby wave train from the North Atlantic to the Iranian Plateau and Tibetan Plateau, traversing over the Eurasian and Ural mountains. However, this wave train had minimal direct influence on East China (Fig. 4c). Therefore, the study did not specifically address the role of SST change over the North Atlantic. Instead, the focus was on the Pacific SST change and its impact on the interdecadal change in summer precipitation over East China around 1760 A.D.

Through sensitivity experiments of CESM-LME using single forcing, we were able to investigate the individual impacts of external forcing factors such as greenhouse gases, solar radiation, orbital parameters, land use, and volcanic activity on the positive PDO phase change around 1760 A.D. The ensemble mean of each sensitivity

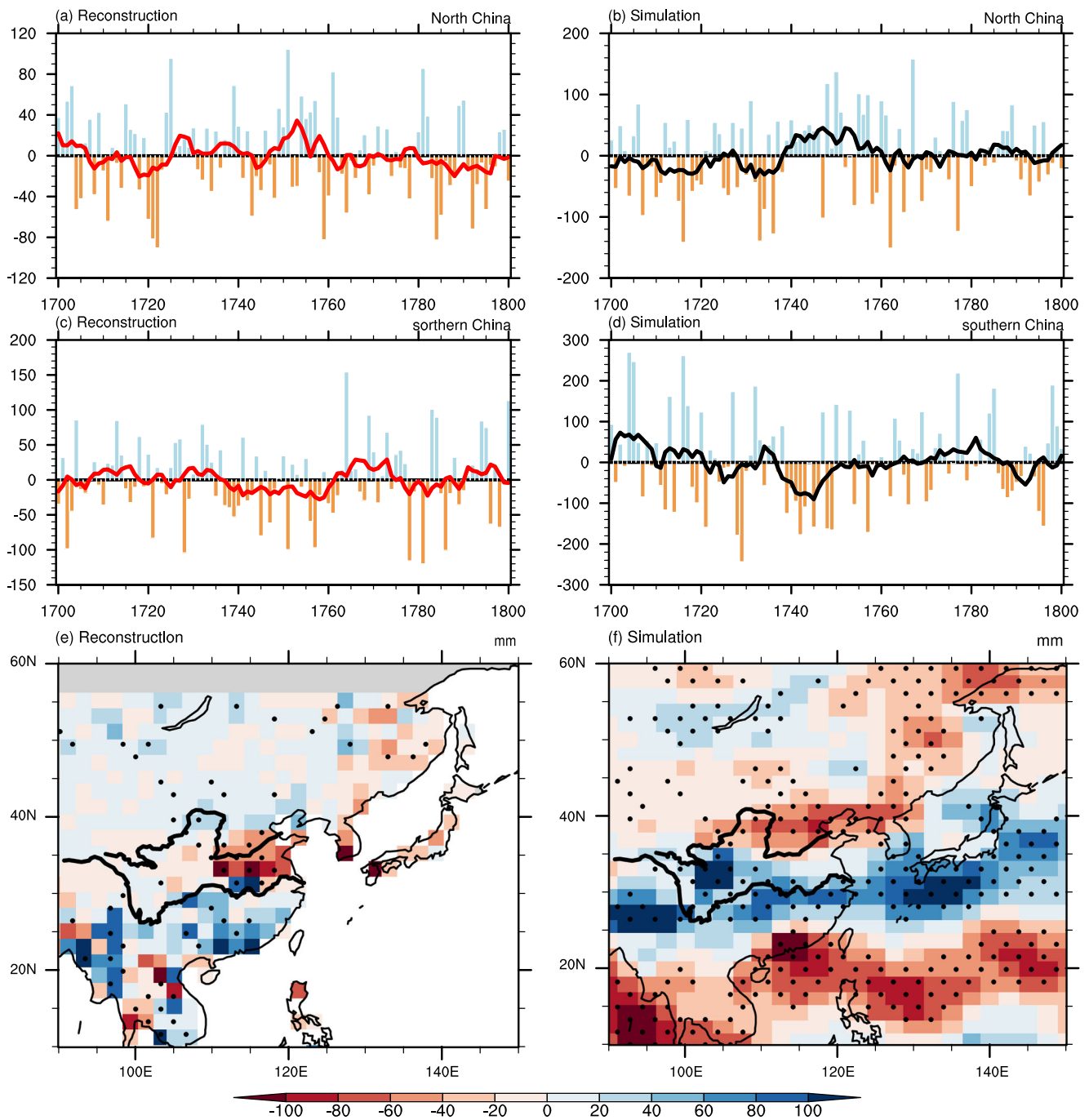


Fig. 1 | Comparison of the summer total precipitation (JJA, unit: mm) between the reconstruction of Shi et al.⁴¹ (left panel) and the simulation using full-forcing ensemble member 001 of CESM-LME (right panel) in North China and southern China during 18th century. a–d Annual and the 9-point moving average detrended annual results of summer total precipitation anomaly in North China and southern

China. **e** The difference of summer total precipitation in East Asia between 1746–1760 A.D. and 1761–1775 A.D. based on reconstruction⁴¹. **f** Same as **e** but using full-forcing ensemble member 001 of CESM-LME. The dot in (**e**) and (**f**) represents the difference is significant at a 95% confidence level.

experiment, roughly excluding simulated internal variability⁶⁵, provides an approximation of the influence of the external forcing, although the ensemble number remains limited. When considering all forcing factors together, there was a transition to a positive phase (Supplementary Figures 12f and 13f), accompanied by larger interdecadal cooling in the interior North Pacific Ocean than in the subpolar North Pacific and the ocean along the coast of North America after 1760 A.D. (Fig. 5n). Thus the external forcing greatly contributed to the PDO-like SST change at that time (Figs. 4a and 5l). The interdecadal SST variation pattern over the Pacific, influenced by all forcing factors after 1760 A.D., can be

largely explained by volcanic forcing (Fig. 5m and Supplementary Figure 12e), with other forcings playing a somewhat lesser role (Supplementary Figure 12). Furthermore, under the influence of all forcings, North China experienced interdecadal drier conditions, whilst Southern China experienced wetter ones (Supplementary Figure 14e). These changes in summer climate could be simulated solely by volcanic activity (Supplementary Figure 14f). Driven by volcanic activity, the ensemble mean of five volcanic-only simulations (Supplementary Figure 15e) revealed a sudden decrease in the net solar flux at the top of the atmosphere after 1760 A.D. This drop was also observed in each individual ensemble of

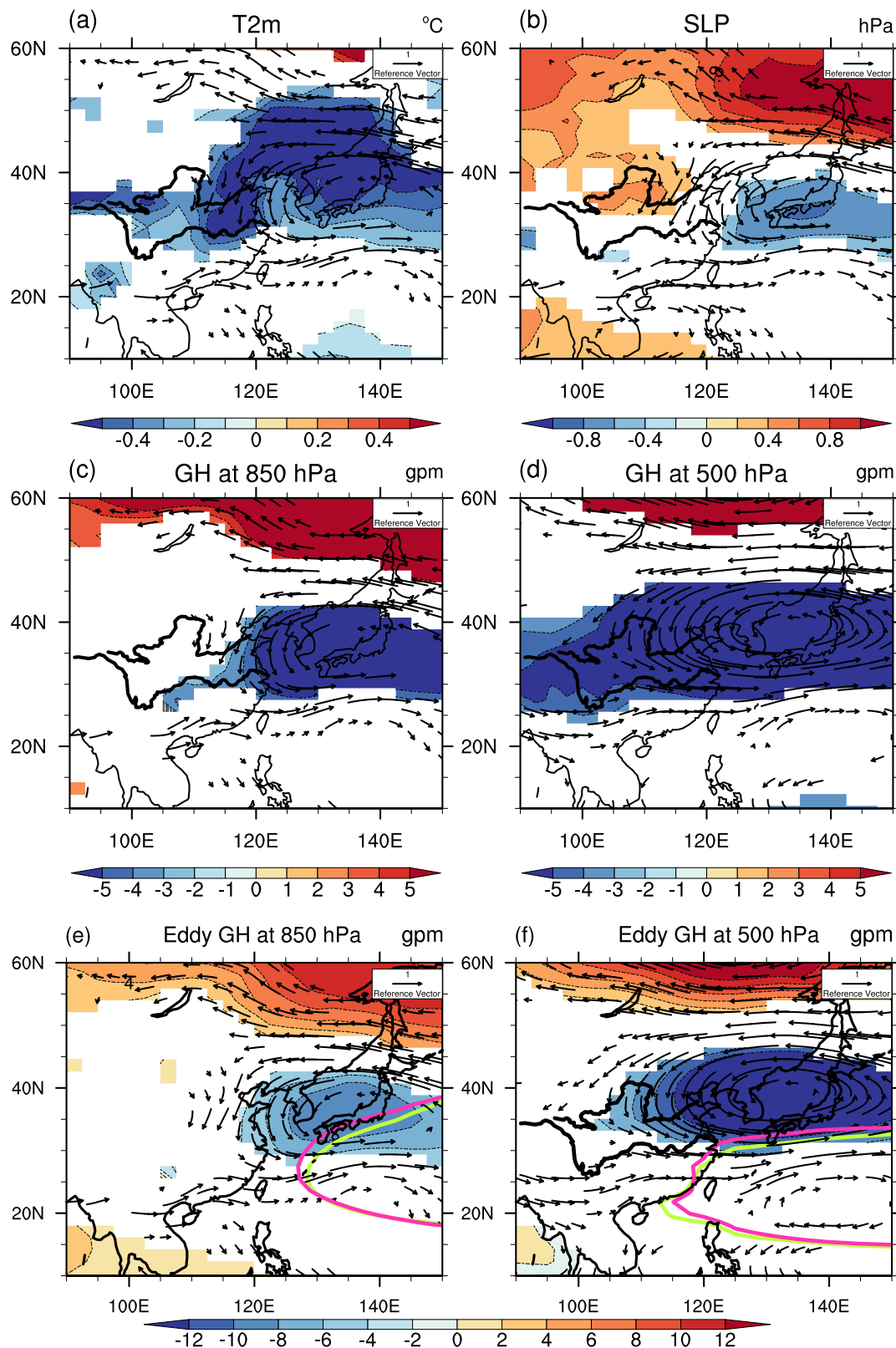


Fig. 2 | Simulated difference in summer circulation between 1761–1775 A.D. and 1746–1760 A.D. based on full-forcing ensemble member 001 of CESM-LME. a Surface 2 m air temperature (T2m, shading, unit: °C) and wind at 850 hPa (arrow, unit: m s^{-1}), both are significant at 90% confidence level. **b** Sea level pressure (SLP, shading, unit: hPa) and wind at 850 hPa (arrow, unit: m s^{-1}), both are significant at 90% confidence level. **c** Geopotential height at 850 hPa (shading, unit: geopotential meter, gpm) and wind at 850 hPa (arrow, unit: m s^{-1}), both are

significant at 90% confidence level. **d** Same as (c), for geopotential height and wind at 500 hPa. **e** Eddy geopotential height at 850 hPa (shading, unit: geopotential meter, gpm) and wind at 850 hPa (arrow, unit: m s^{-1}), both are significant at 95% confidence level. **f** Same as (e), but at 500 hPa. The pink and green color contour lines represent zero eddy geopotential height during 1746–1760 A.D. and 1761–1775 A.D., respectively.

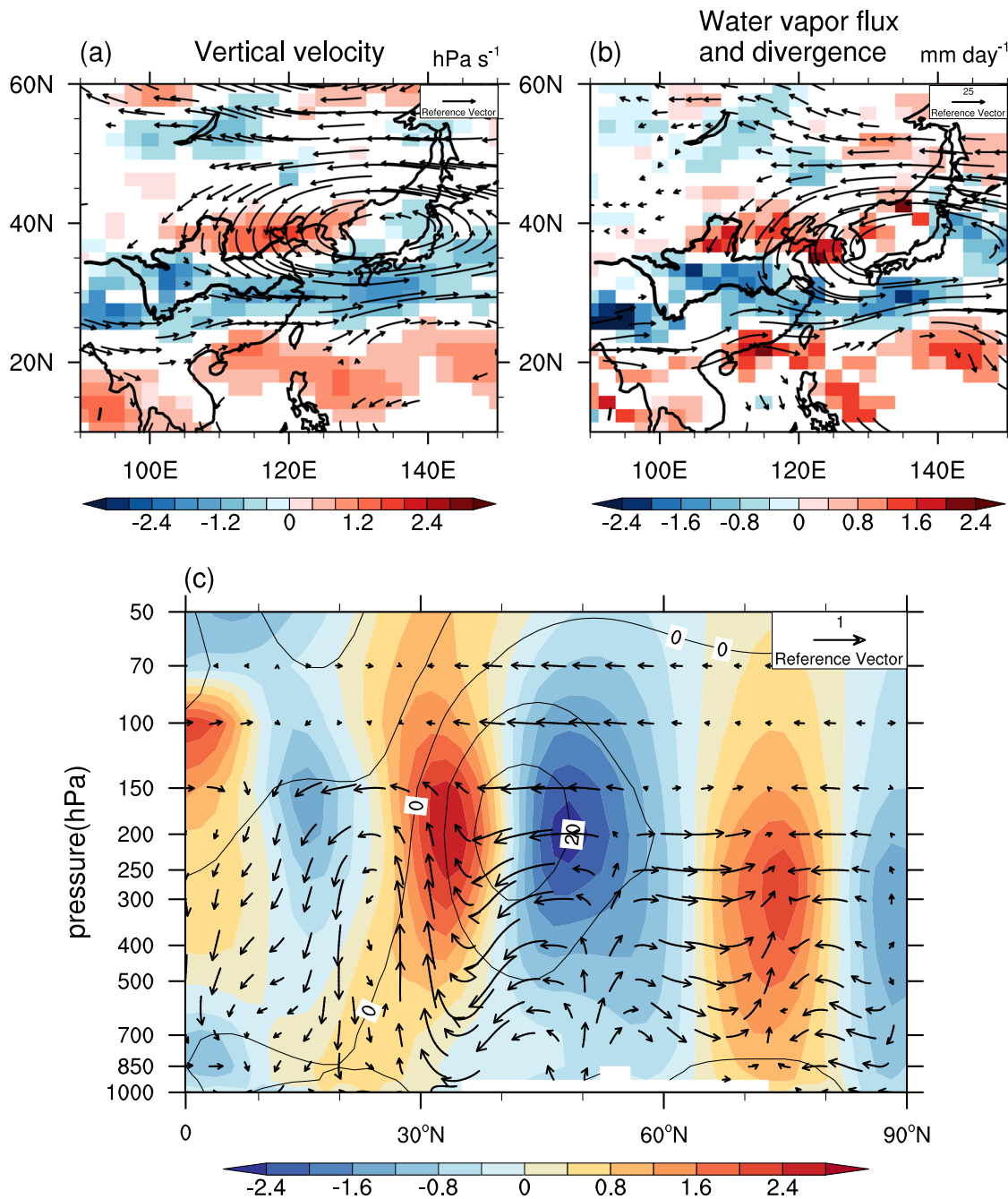


Fig. 3 | Simulated differences of vertical velocity, water vapor transport and westerly circulation in summer between 1761–1775 A.D. and 1746–1760 A.D. based on full-forcing ensemble member 001 of CESM-LME. a Vertical velocity (shading, unit: hPa s⁻¹) and wind at 500 hPa (arrow, unit: m s⁻¹), both are significant at 95% confidence level. **b** Water vapour flux (arrow, unit: kg m⁻¹ s⁻¹) and its divergence,

both are significant at 95% confidence level. **c** Latitude-pressure profile of the zonal wind averaged over 100°E–125°E (shading, unit: m s⁻¹). The contours represent the climatological zonal mean circulation (unit: m s⁻¹) during 1746–1760 A.D. Black arrow represents the composite field of meridional wind (unit: m s⁻¹) and vertical velocity (unit: 0.01 Pa s⁻¹).

the full forcing (Supplementary Figure 16), as well as in their ensemble means (Supplementary Figure 15f), while not in sensitivity experiments driven by other forcing alone (Supplementary Figures 15a–d). In response to volcanic-induced radiative cooling, global cooling patterns over decadal timescales occur unevenly through the ocean dynamic thermostat mechanism and land-sea thermal contrast^{10,42,66}. Consequently, the zonal and/or meridional SST gradients can be modified. These alterations, combined with air-sea feedback, have the potential to induce decadal East Asian climate changes^{8,67}. Therefore, volcanic forcing appears to have played a significant role in the interdecadal variation of PDO-like SST and the summer climate in East Asia around

1760 A.D. Reconstructions and simulations both provide strong evidence supporting the idea that the volcanic forcing could shape the PDO variation and induce the interdecadal climate change^{10,42,68,69}. These volcanic events have far-reaching impacts on the tropical and mid-latitude Pacific Ocean by affecting various atmospheric and oceanic processes^{42,66,70,71}, leading to both immediate and delayed responses^{67,71,72}. Additionally, they can exert a notable influence on the East Asian summer monsoon, interacting with internal climate variability^{44,66}. Consistently, sensitivity experiments with single forcing have shown that volcanic activity is a major external forcing factor contributing to the interdecadal change in PDO-like SST (Fig. 5m) and the variation of

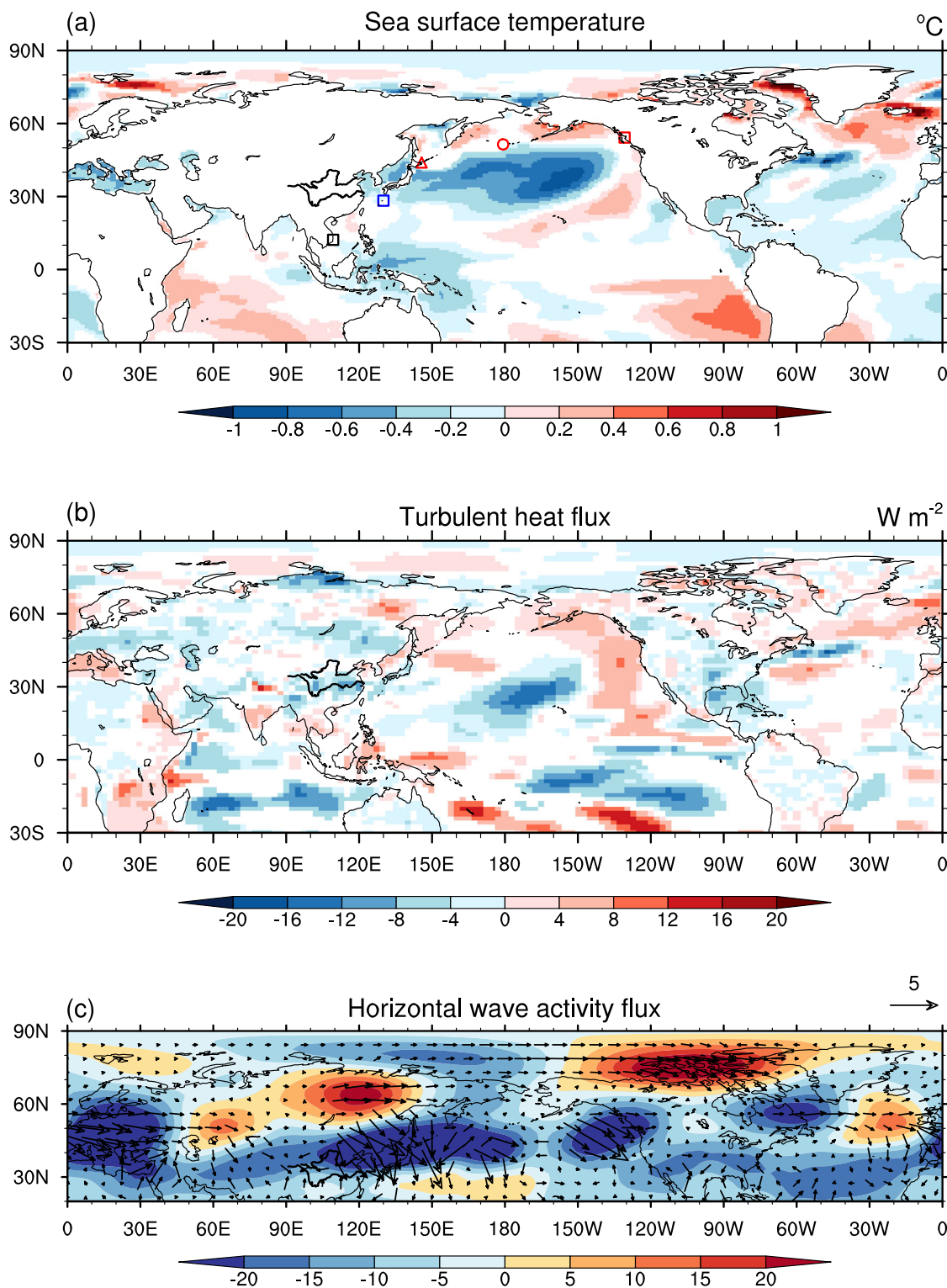
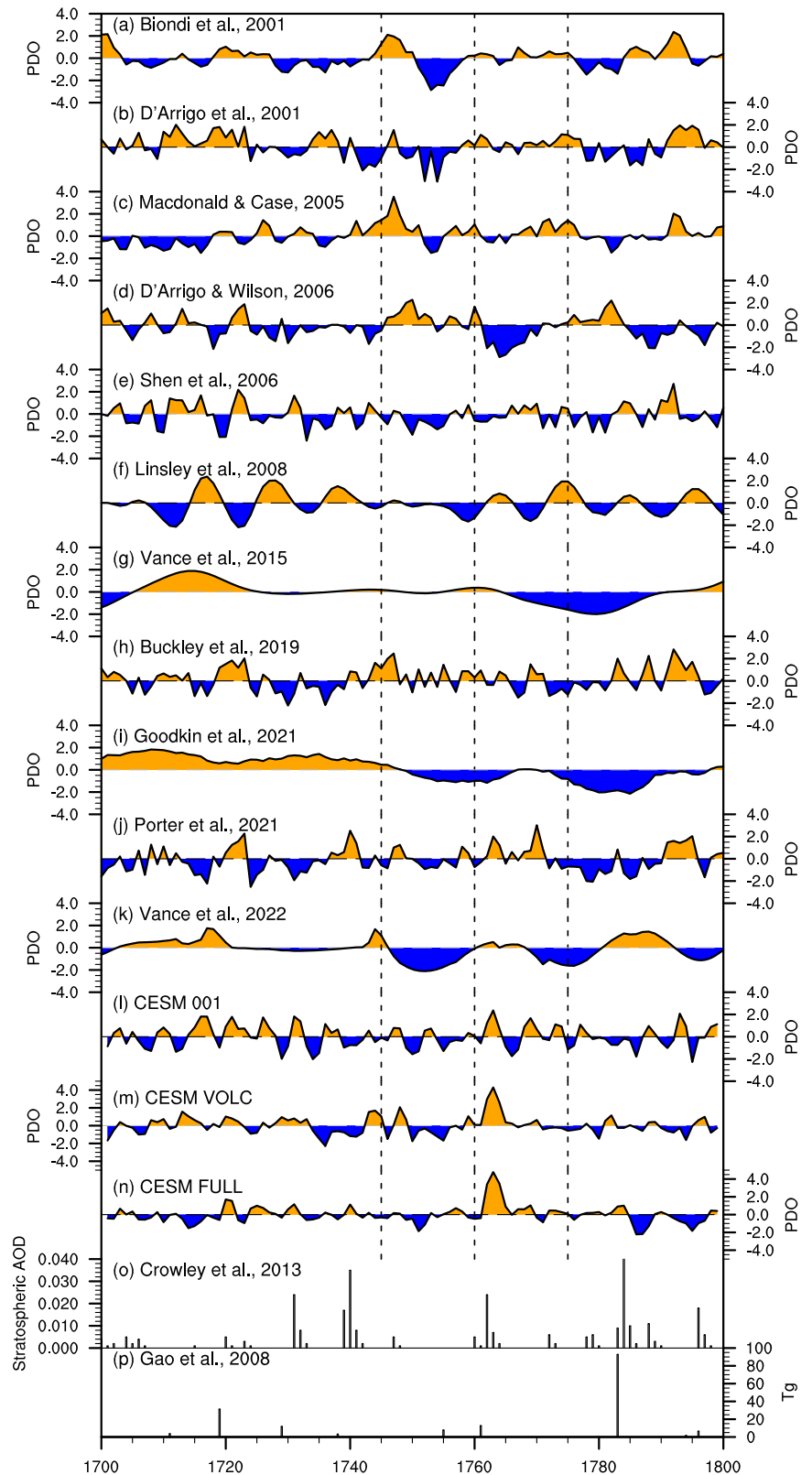


Fig. 4 | Simulated differences of sea surface temperature, turbulent heat flux, and wave activity flux in summer between 1761–1775 A.D. and 1746–1760 A.D. based on full-forcing ensemble member 001 of CESM-LME. a Sea surface temperature (SST, shading, unit: °C, significant at 90% confidence level). Red triangle, circle, and box represent the locations of the reconstruction sites in Kunashir island, Amchitka island (North Pacific), and Tree Nob islands (Northeast Pacific), respectively. They indicate an increase in reconstructed sea surface temperature (SST). Blue box represents the location of the reconstruction site in the Northern

Ryukyus (subtropical Western North Pacific), indicating a decrease of the reconstructed SST. Black box represents the location of the reconstruction site in the South China Sea, showing little change of the reconstructed SST. **b** Turbulent heat flux (the sum of surface sensible heat flux and latent heat flux, shading, unit: $W m^{-2}$, significant at 90% confidence level). **c** 30 years summer horizontal wave activity flux (arrow, unit: $m^2 s^{-2}$) and geopotential height anomaly (shading, unit: gpm) at 200 hPa during 1746–1775 A.D.

Fig. 5 | Comparisons of the reconstructed and simulated PDO index and volcanic activities during the 18th century. a–k The reconstructed PDO index. **l** The simulated PDO index by full-forcing ensemble member 001 of CESM-LME. **m** Same as **l**, but for the ensemble mean of 5 volcanic sensitivity experiments. **n**, Same as **l**, but for the ensemble mean of 11 full-forcing experiments. **o** Reconstructed global average volcanic aerosol optical depth (AOD) at 550 nm⁷³. **p** Global total stratospheric sulfate aerosol injection⁷⁴.



the East Asian summer precipitation around 1760 A.D. (Supplementary Figure 14f).

The reconstructions provide support for volcanic activities both preceding and following the year 1760 A.D. However, there are discrepancies among various studies regarding the specific intensity and frequency of volcanic events^{73,74}. Some studies suggest the occurrence of high-impact

volcanic eruptions in the Philippines in 1754 A.D.⁷⁵ and in the Katla volcanic system in South Iceland in 1755 A.D.⁷⁶. Furthermore, additional evidence indicates the likelihood of a moderate-to-large volcanic eruption event (with a volcanic explosivity index of 4) in Mexico around 1760 A.D., lasting for approximately 15 years until 1774 A.D.^{77,78}. The noteworthy influence of volcanic forcing on the phase shift of the PDO after 1760 A.D. is

underscored in Fig. 5m. Despite the relatively modest level of specified volcanic forcing around 1760 A.D. in CESM-LME, its effect remains notably pronounced (Fig. 5p). This could potentially be attributed to a more pronounced climate response triggered by the occurrence of volcanic double eruptions in relatively close succession, specifically in 1755 A.D. and 1761 A.D. The occurrence of double or clustered volcanic eruptions, even if they are relatively small to moderate, could have significant and long-lasting climate impacts. The occurrence of double or clustered volcanic eruptions, even if they are relatively small to moderate, could have significant and long-lasting climate impacts. This was observed during events such as those that occurred around 536 and 540 A.D.^{68,79}, in the early 19th century⁸⁰, and more recently⁸¹. Thus, it is likely that the moderate volcanic eruption around 1760 A.D. may have caused additional cooling, building upon the previous volcanic activity in 1755 A.D.

It is important to acknowledge that our understanding of past decadal climate change is still limited by the uncertainties inherent in PDO reconstructions. The variation of PDO could modulate the regional climate patterns, including precipitation, temperature, and hydrology. To reconstruct the PDO in historical periods, researchers utilize climate proxies from regions known to be sensitive to PDO variations^{54,60}. By establishing a relationship between these proxies and the PDO based on instrumental data from a given period, it becomes possible to reconstruct the PDO index in the past. PDO reconstruction involves uncertainties mainly stemming from the two main factors: the use of different records or proxies, and uncertainties associated with the relationship between proxies and the PDO during different climatic regimes. On the one hand, the PDO could be reconstructed from tree rings^{54,55,60,64}, drought/flood index derived from historical documents⁶³, coral oxygen isotope records⁵⁷, SST proxy⁶², ice core oxygen isotope records around the Pacific basin⁵⁸, and sea-salt records from East Antarctica^{56,59}. The inherent unreliability and multiple interpretations of proxy data could influence the accuracy of the PDO reconstruction. For example, tree ring records could be influenced by both temperature and precipitation⁵⁴. On the other hand, the relationship between climate proxies and the PDO based on instrumental measurements is not always reliable due to differences in external forcing between historical and modern periods. This can lead to variations in the influence of the PDO on climate patterns and regional intensities during different climate regimes. As a result, PDO reconstructions from different regions may not always be consistent. Besides, simulation uncertainties arising from initial perturbations and internal variability can affect the exact temporal and spatial patterns of decadal climate changes⁸². These uncertainties encompass variations in SST as well as associated circulation and precipitation patterns. The reconstructed SST and PDO index generally support a positive phase PDO-like SST change around 1760 A.D. In comparison, only a subset of the CESM-LME ensembles, including ensembles 001, 004, 006, 007, 009, and 013, simulated the positive phase PDO-like SST change, despite they shared the identical external forcing (Supplementary Figure 17). Among the above six ensembles, 001, 004, and 006 reproduced the positive phase PDO-like SST change around 1760 A.D., while 007, 009, and 013 simulated earlier transitions. Similar as ensemble 001, 006 also simulated the pattern of “southern flooding and northern drought” in the mid-18th century, but located slightly to the south (Supplementary Figure 4), along with a geopotential height anomaly and anomalous circulation center that was also located more to the south (Supplementary Figure 18). Unlikely, ensemble 004 simulated a drier condition in East China, with a larger magnitude in North China than in the southern China (Supplementary Figure 4). Uncertainties arising from the simulations could not be neglected. In addition, the reconstruction of volcanic activity and the performance of the model introduce uncertainties that can influence the assessment of the climate effect of volcanic forcing around 1760 A.D. The volcanic activity during the last millennium still carries uncertainties¹⁰. In comparison to other reconstructions⁷³ (Fig. 5o), the volcanic forcing events around 1760 A.D. incorporated into the CESM-LME model are comparatively less frequent⁷⁴ (Fig. 5p). It is worth noting that the impact of volcanic forcing is likely to be more pronounced if the model includes more frequent volcanic

forcing events after 1760 A.D., as suggested by other evidence^{68,83}. Accurate reconstruction of volcanic activity, along with appropriate specification in climate models, is crucial for effectively reproducing the associated climate effects and subsequent decadal climate changes. To enhance the reliability of decadal simulations in the past or predictions for the future, it is crucial to prioritize the investigation of volcanic activity and the improvement of model performance when simulating the climate impacts of volcanoes^{32,84–88}.

In summary, we analyzed the characteristics and underlying mechanism of the interdecadal climate change in precipitation in East China in the mid-18th century, comparing model simulation and reconstruction. The reconstruction evidence indicates that around 1760 A.D., the summer precipitation in East China experienced an interdecadal transition, characterized by decrease in North China and increase in southern China, resembling the pattern of “southern flooding and northern drought”. CESM-LME ensemble member 001 was able to simulate the interdecadal transition, although the simulated magnitude of the changes was relatively small. The interdecadal variation of summer precipitation in East China in the mid-18th century was associated with the positive phase PDO-like SST change around 1760 A.D., as indicated by both simulation and reconstructions. Corresponding to such sea surface temperature anomalies, the SST in the subtropical regions of the Western North Pacific decreased, leading to weakened convection in the Philippine Sea. These triggered an East Asia-Pacific pattern teleconnection wave train, resulting in the “positive-negative-positive” geopotential height anomaly from south to north in East Asia. This atmospheric anomaly pattern influenced the interdecadal transition of summer precipitation in East China during the mid-18th century. Furthermore, the occurrence of double or clustered volcanic eruptions is believed to have had a significant impact on shifting the phase of the PDO and influencing the decadal summer climate over East China during the mid-18th century. This study highlights the importance of considering external influences, specifically volcanic eruptions, in simulations of past millennia and projections of future climate change over the coming decades. By incorporating these external factors in simulations and improving model performance, we can enhance our understanding of decadal climate change in the past and refine our predictions for the future.

Methods

Data

The reconstructed summer precipitation (including June, July, and August) in East Asia was from Shi et al.⁴¹. The data has a spatial resolution of $2^\circ \times 2^\circ$ and is based on a comprehensive analysis of 453 tree-ring records and 71 historical documents. To select a relatively reasonable simulation, a comparison of the performance of the simulated summer precipitation was made with 13 ensemble experiments from the Community Earth System Model Last Millennium Ensemble (CESM-LME)⁸⁹ (Supplementary Figures 2–6). These experiments were run with CESM1.1, incorporating most relevant forcing factors, as described in Otto-Bliesner et al.⁸⁹. CESM1.1 consists of the atmospheric component of Community Atmosphere Model Version 5 with a resolution of $2.5^\circ \times 1.875^\circ$, and the ocean and sea ice components with an approximate resolution of 1° ⁸⁹. In addition to the CESM-LME, ten other model outputs from the Paleoclimate Modeling Intercomparison Project Phase 3 (PMIP3) were utilized. These simulations cover the period from 850 to 1850 A.D. and incorporate various factors, including total solar irradiance, volcanic activity, orbital parameters, greenhouse gas emissions, and land use and land cover⁸⁹. The results of these simulations are presented in Supplementary Figures 7–9.

Methodology

To identify the sudden interdecadal shift in reconstructed precipitation in East China, a sliding t-test was conducted (see Supplementary Figure 1). This statistical method allows for the detection of significant changes in the precipitation pattern over time. To assess the model's capability to reproduce the interdecadal fluctuations in precipitation during the 18th century in East China, the correlation between each individual ensemble member from the full forcing experiments and the reconstructed precipitation

sequence was examined using sliding correlation. The PDO index is defined as the low-pass filtered primary components of winter SST over the North Pacific using a moving average over a period of nine years. In this study, the wave activity flux has been utilized to assess the energy propagation of the stationary Rossby waves⁹⁰.

Data availability

The data used in this manuscript is free to get. The CESM-LME output is available from <https://www.earthsystemgrid.org/>. The reconstructed precipitation is available in <https://www.ncei.noaa.gov/access/paleo-search/study/24391>. The reconstructed PDO index and SST are available from National Centers for Environmental Information. The volcanic forcing of Gao et al.⁷⁴ is available from <https://climate.envsci.rutgers.edu/TV12/>. The volcanic forcing of Crowley et al.⁷³ is available from <https://www.ncei.noaa.gov/access/paleo-search/study/14168>.

Code availability

The NCAR Command Language (NCL; <http://www.ncl.ucar.edu/>) codes for data analysis and figures generation are available upon request from the corresponding author X. L.

Received: 24 November 2023; Accepted: 11 May 2024;

Published online: 29 May 2024

References

- Boer, G. J. et al. The Decadal Climate Prediction Project (DCPP) contribution to CMIP6. *Geosci. Model Dev.* **9**, 3751–3777 (2016).
- Zhou, T. & Wu, B. Decadal Climate Prediction: Scientific Frontier and Challenge. *Adv. Earth Sci.* **32**, 331–341 (2017).
- Jiang, D., Si, D. & Lang, X. Evaluation of East Asian Summer Climate Prediction from the CESM Large-Ensemble Initialized Decadal Prediction Project. *J. Meteorol. Res.* **34**, 252–263 (2020).
- Ding, Y. et al. Interdecadal and Interannual Variabilities of the Asian Summer Monsoon and Its Projection of Future Change. *Chin. J. Atmos. Sci.* **37**, 253–280 (2013).
- Ding, Y., Wang, Z. & Sun, Y. Inter-decadal variation of the summer precipitation in East China and its association with decreasing Asian summer monsoon. Part I: Observed evidences. *Int. J. Climatol.* **28**, 1139–1161 (2008).
- Ding, Y., Sun, Y., Wang, Z., Zhu, Y. & Song, Y. Inter-decadal variation of the summer precipitation in China and its association with decreasing Asian summer monsoon Part II: Possible causes. *Int. J. Climatol.* **29**, 1926–1944 (2009).
- Zhu, Y., Wang, H., Ma, J., Wang, T. & Sun, J. Contribution of the phase transition of Pacific Decadal Oscillation to the late 1990s' shift in East China summer rainfall. *J. Geophys. Res. Atmos.* **120**, 8817–8827 (2015).
- Wang, T., Ottera, O. H., Gao, Y. Q. & Wang, H. J. The response of the North Pacific Decadal Variability to strong tropical volcanic eruptions. *Clim. Dyn.* **39**, 2917–2936 (2012).
- Zhang, L. & Delworth, T. L. Simulated Response of the Pacific Decadal Oscillation to Climate Change. *J. Clim.* **29**, 5999–6018 (2016).
- Mann, M. E., Steinman, B. A., Brouillette, D. J. & Miller, S. K. Multidecadal Climate Oscillations during the past millennium driven by volcanic forcing. *Science* **371**, 1014–1019 (2021).
- Dai, Z. Q. et al. Atlantic Multidecadal Variability Response to External Forcing during the Past Two Millennia. *J. Clim.* **35**, 4503–4515 (2022).
- Qin, Y. M. et al. Assessing the Modern Multi-Decadal Scale Aridification Over the Northern China From a Historical Perspective. *J. Geophys. Res. Atmos.* **127**, e2021JD035622 (2022).
- He, C. F. et al. Tropical Atlantic multidecadal variability is dominated by external forcing. *Nature* **622**, 521–527 (2023).
- Mantua, N., Hare, S., Zhang, Y., Wallace, J. & Francis, R. A Pacific Interdecadal Climate Oscillation with Impacts on Salmon Production. *Bull. Am. Meteorol. Soc.* **78**, 1069–1079 (1997).
- Tang, M. & Lü, J. The Inter-decadal Mode of the Summer Monsoon Rainfall in East Asia and Its Association with Pacific Decadal Oscillation. *Meteorol. Mon.* **33**, 88–95 (2007).
- Liu, Y., Sun, X. & Yang, X.-Q. Stage-dependent influence of PDO on interdecadal summer precipitation anomalies in eastern China. *Clim. Dyn.* **61**, 2071–2084 (2023).
- Sun, B. et al. How does Mei-yu precipitation respond to climate change? *Natl Sci. Rev.* **10**, nwad246 (2023).
- Huang, R., Liu, Y. & Feng, T. Interdecadal change of summer precipitation over Eastern China around the late-1990s and associated circulation anomalies, internal dynamical causes. *Chin. Sci. Bull.* **58**, 1339–1349 (2013).
- Qian, C. & Zhou, T. J. Multidecadal Variability of North China Aridity and Its Relationship to PDO during 1900–2010. *J. Clim.* **27**, 1210–1222 (2014).
- Yu, L., Furevik, T., Otterå, O. H. & Gao, Y. Modulation of the Pacific Decadal Oscillation on the Summer Precipitation over East China: a comparison of observations to 600-years control run of Bergen Climate Model. *Clim. Dyn.* **44**, 475–494 (2015).
- Si, D. & Ding, Y. Oceanic Forcings of the Interdecadal Variability in East Asian Summer Rainfall. *J. Clim.* **29**, 7633–7649 (2016).
- Xu, P. Q., Wang, L., Chen, W., Feng, J. & Liu, Y. Y. Structural Changes in the Pacific-Japan Pattern in the Late 1990s. *J. Clim.* **32**, 607–621 (2019).
- Si, D., Jiang, D. & Ding, Y. Synergistic Impacts of the Atlantic and Pacific Oceans on Interdecadal Variations of Summer Rainfall in Northeast Asia. *J. Meteorol. Res.* **35**, 844–856 (2021).
- Ding, Q. & Wang, B. Circumglobal Teleconnection in the Northern Hemisphere Summer. *J. Clim.* **18**, 3483–3505 (2005).
- Zhang, Z., Sun, X. & Yang, X.-Q. Understanding the Interdecadal Variability of East Asian Summer Monsoon Precipitation: Joint Influence of Three Oceanic Signals. *J. Clim.* **31**, 5485–5506 (2018).
- Ge, Y., Miao, J., Lang, X., Si, D. & Jiang, D. Combined Impacts of the Pacific Decadal Oscillation and Atlantic Multidecadal Oscillation on Summer Precipitation in Eastern China During the Medieval Climate Anomaly and Little Ice Age. *J. Geophys. Res. Atmos.* **128**, e2023JD038920 (2023).
- Kwon, M., Jhun, J.-G. & Ha, K.-J. Decadal change in east Asian summer monsoon circulation in the mid-1990s. *Geophys. Res. Lett.* **34**, L21706 (2007).
- Lapp, S. L., St Jacques, J. M., Barrow, E. M. & Sauchyn, D. J. GCM projections for the Pacific Decadal Oscillation under greenhouse forcing for the early 21st century. *Int. J. Climatol.* **32**, 1423–1442 (2012).
- Smith, D. M. et al. Role of volcanic and anthropogenic aerosols in the recent global surface warming slowdown. *Nat. Clim. Change* **6**, 936–940 (2016).
- Hua, W., Dai, A. & Qin, M. Contributions of Internal Variability and External Forcing to the Recent Pacific Decadal Variations. *Geophys. Res. Lett.* **45**, 7084–7092 (2018).
- Li, S. J. et al. The Pacific Decadal Oscillation less predictable under greenhouse warming. *Nat. Clim. Change* **10**, 30–34 (2020).
- Power, S. et al. Decadal climate variability in the tropical Pacific: Characteristics, causes, predictability, and prospects. *Science* **374**, ea9165 (2021).
- Sun, W., Wang, B., Liu, J. & Dai, Y. Recent Changes of Pacific Decadal Variability Shaped by Greenhouse Forcing and Internal Variability. *J. Geophys. Res. Atmos.* **127**, e2021JD035812 (2022).
- Ma, Y., Yuan, N., Dong, T. & Dong, W. On the Pacific Decadal Oscillation Simulations in CMIP6 Models: A New Test-Bed from Climate Network Analysis. *Asia. Pac. J. Atmos. Sci.* **59**, 17–28 (2023).
- Geng, T., Yang, Y. & Wu, L. On the Mechanisms of Pacific Decadal Oscillation Modulation in a Warming Climate. *J. Clim.* **32**, 1443–1459 (2019).
- Steffen, W., Grinevald, J., Crutzen, P. & McNeill, J. The Anthropocene: conceptual and historical perspectives. *Philos. Trans. R. Soc. A* **369**, 842–867 (2011).

37. Smith, B. D. & Zeder, M. A. The onset of the Anthropocene. *Anthropocene* **4**, 8–13 (2013).
38. Pei, L., Yan, Z. & Yang, H. Multidecadal variability of dry/wet patterns in eastern China and their relationship with the Pacific Decadal Oscillation in the last 413 years. *Chin. Sci. Bull.* **60**, 97–108 (2015).
39. Peng, Y., Shen, C., Cheng, H. & Xu, Y. Simulation of the Interdecadal Pacific Oscillation and its impacts on the climate over eastern China during the last millennium. *J. Geophys. Res. Atmos.* **120**, 7573–7585 (2015).
40. Yang, K. & Jiang, D. Interannual climate variability change during the Medieval Climate Anomaly and Little Ice Age in PMIP3 last millennium simulations. *Adv. Atmos. Sci.* **34**, 497–508 (2017).
41. Shi, H., Wang, B., Cook, E. R., Liu, J. & Liu, F. Asian Summer Precipitation over the Past 544 Years Reconstructed by Merging Tree Rings and Historical Documentary Records. *J. Clim.* **31**, 7845–7861 (2018).
42. Sun, W., Liu, J., Wang, B., Chen, D. & Gao, C. Pacific multidecadal (50–70 year) variability instigated by volcanic forcing during the Little Ice Age (1250–1850). *Clim. Dyn.* **59**, 231–244 (2022).
43. Hau, N.-X., Sano, M., Nakatsuka, T., Chen, S.-H. & Chen, I. C. The modulation of Pacific Decadal Oscillation on ENSO-East Asian summer monsoon relationship over the past half-millennium. *Sci. Total Environ.* **857**, 159437 (2023).
44. Jiang, S. et al. Increased effective radiative forcing enhanced the modulating effect of Pacific Decadal Oscillation on late Little Ice Age precipitation in the Jiang-Huai region, China. *Clim. Dyn.* **61**, 4173–4183 (2023).
45. Xue, J. et al. The combined influences of Solar Radiation and PDO on Precipitation over Eastern China during the last millennium. *Clim. Dyn.* **60**, 1137–1150 (2023).
46. Yang, K. et al. The Asian–Pacific oscillation over the past millennium in PMIP3 and PMIP4. *Quat. Sci. Rev.* **301**, 107918 (2023).
47. Edge, D. C. et al. A Multicentennial Proxy Record of Northeast Pacific Sea Surface Temperatures From the Annual Growth Increments of *Panopea generosa*. *Paleoceanogr. Paleoclimatol.* **36**, e2021PA004291 (2021).
48. Williams, B. et al. North Pacific twentieth century decadal-scale variability is unique for the past 342 years. *Geophys. Res. Lett.* **44**, 3761–3769 (2017).
49. Wiles, G. C. et al. Surface air temperature variability reconstructed with tree rings for the Gulf of Alaska over the past 1200 years. *Holocene* **24**, 198–208 (2014).
50. Winski, D. et al. A 400-Year Ice Core Melt Layer Record of Summertime Warming in the Alaska Range. *J. Geophys. Res. Atmos.* **123**, 3594–3611 (2018).
51. Demezhko, D. Y. & Solomina, O. N. Ground surface temperature variations on Kunashir Island in the last 400 years inferred from borehole temperature data and tree-ring records. *Dokl. Earth Sci.* **426**, 628–631 (2009).
52. Tierney, J. E. et al. Tropical sea surface temperatures for the past four centuries reconstructed from coral archives. *Paleoceanography* **30**, 226–252 (2015).
53. Kawakubo, Y., Alibert, C. & Yokoyama, Y. A Reconstruction of Subtropical Western North Pacific SST Variability Back to 1578, Based on a Porites Coral Sr/Ca Record from the Northern Ryukyus, Japan. *Paleoceanography* **32**, 1352–1370 (2017).
54. Biondi, F., Gershunov, A. & Cayan, D. R. North Pacific Decadal Climate Variability since 1661. *J. Clim.* **14**, 5–10 (2001).
55. D'Arrigo, R., Villalba, R. & Wiles, G. Tree-ring estimates of Pacific decadal climate variability. *Clim. Dyn.* **18**, 219–224 (2001).
56. Vance, T. R., Roberts, J. L., Plummer, C. T., Kiem, A. S. & van Ommen, T. D. Interdecadal Pacific variability and eastern Australian megadroughts over the last millennium. *Geophys. Res. Lett.* **42**, 129–137 (2015).
57. Linsley, B. K., Zhang, P., Kaplan, A., Howe, S. S. & Wellington, G. M. Interdecadal-decadal climate variability from multicoral oxygen isotope records in the South Pacific Convergence Zone region since 1650 A.D. *Paleoceanography* **23**, PA2219 (2008).
58. Porter, S. E., Mosley-Thompson, E., Thompson, L. G. & Wilson, A. B. Reconstructing an Interdecadal Pacific Oscillation Index from a Pacific Basin–Wide Collection of Ice Core Records. *J. Clim.* **34**, 3839–3852 (2021).
59. Vance, T. R. et al. Pacific decadal variability over the last 2000 years and implications for climatic risk. *Commun. Earth Environ.* **3**, 33 (2022).
60. MacDonald, G. M. & Case, R. A. Variations in the Pacific Decadal Oscillation over the past millennium. *Geophys. Res. Lett.* **32**, L08703 (2005).
61. D'Arrigo, R. & Wilson, R. On the Asian expression of the PDO. *Int. J. Climatol.* **26**, 1607–1617 (2006).
62. Goodkin, N. F. et al. Natural and Anthropogenic Forcing of Multi-Decadal to Centennial Scale Variability of Sea Surface Temperature in the South China Sea. *Paleoceanogr. Paleoclimatol.* **36**, e2021PA004233 (2021).
63. Shen, C., Wang, W.-C., Gong, W. & Hao, Z. A Pacific Decadal Oscillation record since 1470 AD reconstructed from proxy data of summer rainfall over eastern China. *Geophys. Res. Lett.* **33**, L03702 (2006).
64. Buckley, B. M. et al. Interdecadal Pacific Oscillation reconstructed from trans-Pacific tree rings: 1350–2004 CE. *Clim. Dyn.* **53**, 3181–3196 (2019).
65. Booth, B. B. B., Dunstone, N. J., Halloran, P. R., Andrews, T. & Bellouin, N. Aerosols implicated as a prime driver of twentieth-century North Atlantic climate variability. *Nature* **484**, 228–232 (2012).
66. Liu, F. et al. Tropical volcanism enhanced the East Asian summer monsoon during the last millennium. *Nat. Commun.* **13**, 3429 (2022).
67. Ning, L. et al. How Do Volcanic Eruptions Influence Decadal Megadroughts over Eastern China? *J. Clim.* **33**, 8195–8207 (2020).
68. Sigl, M. et al. Timing and climate forcing of volcanic eruptions for the past 2,500 years. *Nature* **523**, 543–549 (2015).
69. Shi, F. et al. Interdecadal to Multidecadal Variability of East Asian Summer Monsoon Over the Past Half Millennium. *J. Geophys. Res. Atmos.* **127**, e2022JD037260 (2022).
70. McGregor, S. et al. The Effect of Strong Volcanic Eruptions on ENSO, in *El Niño Southern Oscillation in a Changing Climate*, edited, pp. 267–287 (2020).
71. Pausata, F. S. R., Zhao, Y., Zanchettin, D., Caballero, R. & Battisti, D. S. Revisiting the Mechanisms of ENSO Response to Tropical Volcanic Eruptions. *Geophys. Res. Lett.* **50**, e2022GL102183 (2023).
72. Mehta, V. M., Wang, H. & Mendoza, K. Simulations of three natural decadal climate variability phenomena in CMIP5 experiments with the UKMO HadCM3, GFDL-CM2.1, NCAR-CCSM4, and MIROC5 global earth system models. *Clim. Dyn.* **51**, 1559–1584 (2018).
73. Crowley, T. J. & Unterman, M. B. Technical details concerning development of a 1200 yr proxy index for global volcanism. *Earth Syst. Sci. Data* **5**, 187–197 (2013).
74. Gao, C., Robock, A. & Ammann, C. Volcanic forcing of climate over the past 1500 years: An improved ice core-based index for climate models. *J. Geophys. Res. Atmos.* **113**, D23111 (2008).
75. Delos Reyes, P. J. et al. A synthesis and review of historical eruptions at Taal Volcano, Southern Luzon, Philippines. *Earth Sci. Rev.* **177**, 565–588 (2018).
76. Larsen, G. 3 Katla: Tephrochronology and Eruption History, In A. Schomacker, J. Krüger, K. H. Kjær (Eds.), *The Myrdalsjøkull Ice Cap, Iceland. Glacial Processes, Sediments and Landforms on an Active Volcano*, **13**, 23–49 (2010).
77. Kozak, J. & Cermak, V. Jorullo Volcano, Mexico. *The Illustrated History of Natural Disasters*. Dordrecht: Springer Netherlands (2010).
78. Bregy, J. C. et al. US Gulf Coast tropical cyclone precipitation influenced by volcanism and the North Atlantic subtropical high. *Commun. Earth Environ.* **3**, 164 (2022).
79. Toohey, M., Krüger, K., Sigl, M., Stordal, F. & Svensen, H. Climatic and societal impacts of a volcanic double event at the dawn of the Middle Ages. *Clim. Change* **136**, 401–412 (2016).

80. Fang, S.-W. et al. The Role of Small to Moderate Volcanic Eruptions in the Early 19th Century Climate. *Geophys. Res. Lett.* **50**, e2023GL105307 (2023).
 81. Schmidt, A. et al. Volcanic radiative forcing from 1979 to 2015. *J. Geophys. Res. Atmos.* **123**, 12491–12508 (2018).
 82. Shi, J., Yan, Q. & Wang, H. Timescale dependence of the relationship between the East Asian summer monsoon strength and precipitation over eastern China in the last millennium. *Clim* **14**, 577–591 (2018).
 83. Van Dijk, E. et al. Climatic and societal impacts in Scandinavia following the 536 and 540 CE volcanic double event. *Clim* **19**, 357–398 (2023).
 84. Bethke, I. et al. Potential volcanic impacts on future climate variability. *Nat. Clim. Change* **7**, 799–805 (2017).
 85. Liguori, G., McGregor, S., Arblaster, J. M., Singh, M. S. & Meehl, G. A. A joint role for forced and internally-driven variability in the decadal modulation of global warming. *Nat. Commun.* **11**, 3827 (2020).
 86. Marshall, L. R. et al. Volcanic effects on climate: recent advances and future avenues. *Bull. Volcanol.* **84**, 54 (2022).
 87. Paik, S. et al. Impact of volcanic eruptions on extratropical atmospheric circulations: review, revisit and future directions. *Environ. Res. Lett.* **18**, 063003 (2023).
 88. Wu, X., Yeager, S. G., Deser, C., Rosenbloom, N. & Meehl, G. A. Volcanic forcing degrades multiyear-to-decadal prediction skill in the tropical Pacific. *Sci. Adv.* **9**, eadd9364 (2023).
 89. Otto-Bliesner, B. L. et al. Climate Variability and Change since 850 CE: An Ensemble Approach with the Community Earth System Model. *Bull. Am. Meteorol. Soc.* **97**, 735–754 (2016).
 90. Takaya, K. & Nakamura, H. A Formulation of a Phase-Independent Wave-Activity Flux for Stationary and Migratory Quasigeostrophic Eddies on a Zonally Varying Basic Flow. *J. Atmos. Sci.* **58**, 608–627 (2001).
- manuscript. X. L. thanks Dr. Qing Yan of IAPCAS for providing assistance in drawing.

Author contributions

X.L. conceived the study. G.C. performed most of the analysis and prepared the draft manuscript. X.L. collected the reconstructions and compared model-data. Z.X. and Y.L. contributed to the interpretation of the dynamic analysis. Y.L. and S.S. assisted with the sliding t-test analysis. Z.X. and S.S. assisted with the analysis of the wave activity flux. X.L. and G.C. edited the manuscript with suggestions from Z.X., Y.L., Z.Z., and J.G.

Competing interests

The authors declare no competing interests.

Additional information

Supplementary information The online version contains supplementary material available at <https://doi.org/10.1038/s41612-024-00666-6>.

Correspondence and requests for materials should be addressed to Xiangyu Li.

Reprints and permissions information is available at <http://www.nature.com/reprints>

Publisher's note Springer Nature remains neutral with regard to jurisdictional claims in published maps and institutional affiliations.

Open Access This article is licensed under a Creative Commons Attribution 4.0 International License, which permits use, sharing, adaptation, distribution and reproduction in any medium or format, as long as you give appropriate credit to the original author(s) and the source, provide a link to the Creative Commons licence, and indicate if changes were made. The images or other third party material in this article are included in the article's Creative Commons licence, unless indicated otherwise in a credit line to the material. If material is not included in the article's Creative Commons licence and your intended use is not permitted by statutory regulation or exceeds the permitted use, you will need to obtain permission directly from the copyright holder. To view a copy of this licence, visit <http://creativecommons.org/licenses/by/4.0/>.

© The Author(s) 2024

Acknowledgements

This work was supported by National Natural Science Foundation of China (42125502, 42275047, and 42005042) and National Key R&D Program of China (2018YFA0605602). We acknowledge the CESM Paleoclimate Working Group at NCAR for producing and making available the model output from the CESM1 (CAM5) Last Millennium Ensemble Community Project and supercomputing resources provided by NSF/CISL/Yellowstone. We thank the National Centers for Environmental Information for providing paleoclimatology data from the NOAA/World Data Service. We appreciate the reviewers' constructive comments and contributions to enhancing the